Design and Fabrication of a Novel Microfluidic Nanoprobe

Nicolaie Moldovan, Keun-Ho Kim, and Horacio D. Espinosa, *Fellow, ASME*

***Abstract*—The design and fabrication of a novel microfluidic nanoprobe system are presented. The nanoprobe consists of cantilevered ultrasharp volcano-like tips, with microfluidic capabilities consisting of microchannels connected to an on-chip reservoir. The chip possesses additional connection capabilities to a remote reservoir. The fabrication uses standard surface micromachining techniques and materials. Bulk micromachining is employed for chip release. The microchannels are fabricated in silicon nitride by a new methodology, based on edge underetching of a sacrificial layer, *bird's beak* oxidation for mechanically closing the edges, and deposition of a sealing layer. The design and integration of various elements of the system and their fabrication are discussed. The system is conceived mainly to work as a "nanofountain pen", i.e., a continuously writing upgrade of the dip-pen nanolithography approach. Moreover, the new chip shows a much larger applicability area in fields such as electrochemical nanoprobes, nanoprobe-based etching, build-up tools for nanofabrication, or a probe for materials interactive analysis. Preliminary tests for writing and imaging with the new device were performed. These tests illustrate the capabilities of the new device and demonstrate possible directions for improvement. [1517]**

***Index Terms*—Dip-pen nanolithography, microfluidics, micropipette, nanoprobe.**

I. Introduction

SEVERAL microfluidic nanoprobe techniques have been reported in the literature. These probes possess the capability of delivering or probing fluids at the atto litter volume range, with atomic force microscopy positioning accuracy. A first category is known as "nanopipettes"—sharpened tubules, with outer diameters in the 10–50 nm range, usually obtained by pulling capillaries. They were reportedly used for scanning molecule microscopy [1], scanning ion conductance microscopy [2], fountain pen nanochemistry for chromium etching [3], resist delivery systems for nanolithography [4], and "nanojets" for delivery of plasma-generated radicals for nanopatterning by etching [5]. These tubular nanopipettes are capable of writing or sampling with critical dimensions in the micrometer or upper submicrometer range. Other tubular nanoprobes just contain fluorescent dyes for near field scanning optical microscopy [6], without attempting to exchange materials with the substrates. At the micron scale, we have what is known as "micropipettes", which have lumen sizes in the 1–10 micron range. Applications of micropipettes include injection, motion, and placement of liquids in chemical analysis systems [7], drug delivery or biofluid sampling applications [8]. Major applications of micropipettes are in cell-level physiology experimentation [9], in microdialysis, microvoltametry, and studies of ion transfer across micro-interfaces of two immiscible electrolyte solutions (micro-ITIE's) [10], [11].

A different approach for the delivery of molecular "inks" is the so-called dip-pen nanolithography (DPN) technique [12]–[17], which uses a pre-coated atomic force microscope (AFM) tip to write on substrates using various tailored ink species. Features with size as small as 15 nm have been reported. The ink and substrate have to be chosen to allow a chemical reaction between them during deposition. Several substrate/ink pairs have been reported in the literature, e.g., Au/1-octadecanethiol (ODT) [12], Au/16-mercaptohexadecanoic acid (MHA) [13], Si or GaAs/hexamethyldisilazane (HMDS) [14], and many other materials, including paired proteins and DNA strands [15], [16]. The delivery is surface diffusion-driven along the substrate [17]. The capillary condensation of water between the tip and substrate seems to play an important, but controversial, role in the process [18], [19]. By applying voltage between the tip and substrate and using metal- or semiconductor-containing inks, deposition of various materials such as Pt, Au, Ge, Ag, Cu, and Pd have been reported in a so-called "electrochemical dip-pen nanolithography" approach [20].

A common limitation of the micropipette and DPN approaches is the slowness in writing or sampling capability. Several are the causes for the process slowness: the diffusion or slow flow of fluids; the necessity to re-ink and re-position the probes if the delivered species are exhausted; the limited response time of the electromechanical scanning systems and the necessity to scan large areas with a single probe. To speed up the process, parallel writing is needed. With pulled glass micropipettes, this is hindered by the difficulty to integrate such parts in arrays. In contrast, parallel writing was demonstrated with arrays of micromachined tips—the "Millipede" approach [21], but no ink was delivered, since this is a thermal writing mode. Multiple ink writing in the DPN mode was demonstrated only sequentially, by changing the tips and re-aligning [13], while parallel DPN writing has been experimented, but is limited by the thermal actuation of the cantilevers and the absence of a straightforward ink-replenishing procedure [22], [23]. Integration of microfluidics in arrays of cantilevers and AFM tips remains a challenge. Such integration would eventually allow writing/reading with different inks, thus, rendering a tool to build-up and pattern complex material systems at the

Manuscript received February 15, 2005; revised July 29, 2005. This work was supported by the Nanoscale Science and Engineering Initiative of the National Science Foundation under NSF Award Number EEC-0118025. Subject Editor D. Cho.

The authors are with the Mechanical Engineering, Northwestern University, Evanston, IL 60208 USA (e-mail: espinosa@northwestern.edu).

Digital Object Identifier 10.1109/JMEMS.2005.863701

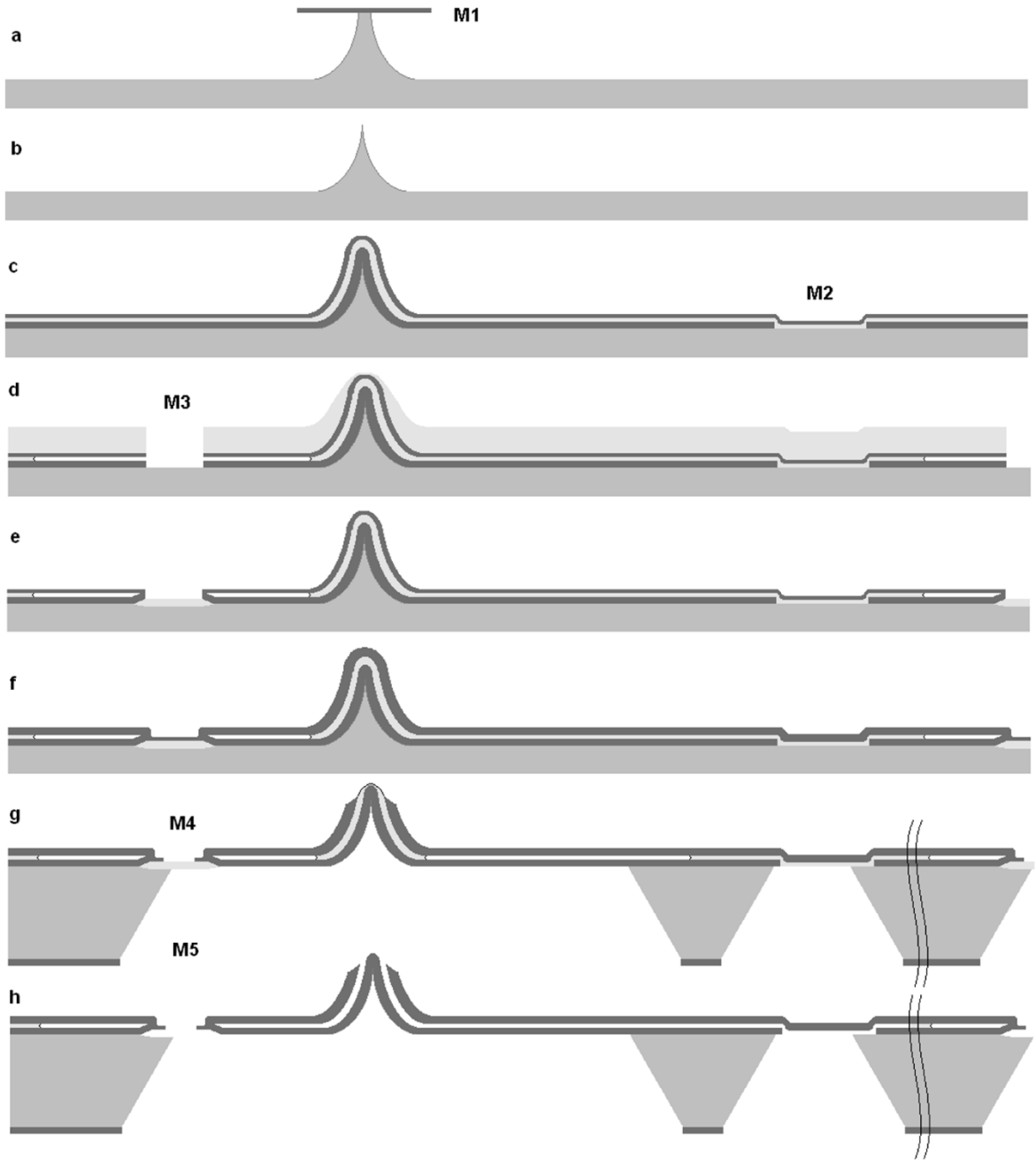

Fig. 1. Fabrication flow chart of microfluidic nanoprobe chip. (a) Fabrication of tip precursors, (b) oxidation sharpening and oxide removal, (c) deposition of Si_3N_4, lithography with mask M2 for defining the reservoir followed by deposition of SiO_2 sacrificial layer and Si_3N_4 microchannel ceiling layer, (d) lithography with mask M3, for delineating the channels, and underetching of SiO_2 for creating the channel lumen, (e) *bird's beak* oxidation for closing the channel sides, (f). deposition of the sealing layer, (g). lithography with mask M4 on top side for delineating the cantilevers, followed by backside lithography with mask M5, for defining the reservoir and chip boundaries, and KOH etching; during the nitride etching step, the tips protrude from the photoresist and start being etched; (h) oxide wet chemical etching for connecting the volcano-tip with the microchannels and releasing the cantilevers and chip. Note that in step (g) the cross section has been slightly shifted to illustrate the channel formation.

nano-scale. Applications of the technology include: nanosensors, combinatorial biochemistry, proteomics, DNA synthesis, nanoelectronics and others. Here we report on a first attempt to establish a technology for integrating microchannels, arrays of AFM cantilevers, microfluidic reservoirs and nanodispensing AFM tips into a complex microfluidic nanoprobe chip. The design and successful microfabrication of chips incorporating a reservoir and five cantilevers, with embedded microchannels connecting the reservoir to specially designed dispensing tips, is reported.

This paper provides an in-depth discussion of the design, micromachining and microfluidics integration issues of the fountain pen chip first reported in [24], [25]. Writing experiments in *fountain pen mode* with molecular ink transport from the reservoir to the tips are also reported. These experiments show that the tips perform well and preserve the dip-pen diffusion-driven writing mode (40 nm line widths). The integration of independent actuation of each cantilever, arraying and multiple ink capabilities are currently under development and will be addressed in forthcoming publications.

TABLE I
GENERAL PARAMETERS OF THE DESIGNED MICROFLUIDIC NANOPROBE CHIP

Tip height	3-8 μm
Cantilever material	Si_3N_4 (LPCVD), with SiO_2 (LTO) core and sacrificial layer
Cantilever freestanding lengths	400 μm, 450 μm, 500 μm, 550 μm, and 600 μm
Cantilever widths	22 μm
Cantilever stiffness	0.05 to 0.5 N/m
Chip size (excluding cantilevers)	2158 μm x 3282 μm
Reservoir size	1240 μm x 1354 μm
Channel cross section	(0.3 to 1) μm x (5 to 7) μm
Chip body material	Si (100), 350-μm-thick, 50 Ωcm p-type

II. GENERAL DESIGN

The design of the microfluidic nanoprobe is driven by the functionality requirements discussed above. One of the major differences between a micropipette writing mode and the DPN writing mode is in the way the ink is delivered to the surface, with direct consequences on pattern size and resolution. In a micropipette writing mode, the capillary lumen is filled with liquid; hence, upon contact with the substrate, there is a reshaping of the meniscus to form an outer liquid droplet surrounding the capillary. This droplet is dragged along the substrate and produces the desired pattern [3]. Thus, the smallest writable features are a function of the lumen size, currently in the micron range. By contrast, in DPN, although a liquid meniscus may eventually form between the tip and substrate due to capillary condensation [26], spot growth dynamics on the substrate suggests diffusion as the driving mechanism for writing [17]. Since the AFM tips so far are always dried before writing, and many of the "inks" are insoluble in water, surface diffusion may be also the ink supplying mechanism along the tip. The capillary condensation meniscus formed between the tip and substrate, if any [18], appears to play a role in constraining the path of the molecules. This mechanism, which defines the DPN writing mode, was proven to result in 15 nm features with 5 nm spacing [12]–[16]. Having these in mind, a first constraint in our design was imposed by the desire to preserve this high resolution DPN writing mode. For this reason, the ultimate ink delivery system requires an AFM tip. However, the supply of ink has to be continuous, to avoid interruptions for replenishing of molecules. Since distances along the chip and cantilevers are in the millimeter range, a liquid source is supposed to be the only one providing good molecular transport. In this scenario, the ink molecules have to be soluble in the ink solvent, the liquid has to be delivered through capillary channels close to the tip apex, but the meniscus has to end prior to reaching the apex of the AFM probe. To avoid the rapid evaporation of the ink solvent, the channels are preferred to be closed along the path from the reservoir to the dispensing tip. Other constrains on the cantilevers are imposed by the requirements to keep their stiffness low (0.03–0.3 N/m), to achieve both normal (writing) and lateral force microscopy (reading) high resolutions, while the tip material should be hard and sufficiently hydrophilic to facilitate molecular transport. Silicon nitride, proven to give good results in DPN experiments, and combinations of silicon nitride and other materials were studied by microfluidic simulations [24] for several possible geometries of the dispensing tips. The results showed that the liquid is driven to fill the microchannels by capillary action. It forms a liquid-air interface at the tip outlet, where a ring-shape aperture of the dispensing tip configures conveniently the meniscus, while preventing a direct wetting of the substrate.

Minimization of processing steps and the usage of common fabrication techniques and materials available in standard microfabrication laboratories are also desirable. The design should also be versatile to permit easy addition of upgrades, such as variation in tip shapes, cantilever stiffness, integration of independent actuation and large-scale arraying capabilities for both the micromechanical parts and the electrical and microfluidic circuitry.

After considering and evaluating several design and fabrication options, a solution based on the processing flowchart presented in Fig. 1 was adopted. The main parameters of the designed microfluidic nanoprobe chip are given in Table I. Several novel fabrication approaches were implemented, which will be discussed in separate sections. A schematic view on the outcome, including the future upgrades are presented in Fig. 2, while a general view on the fabricated chip can be seen in Fig. 3.

The first step in the process is the fabrication of tips, by silicon etching (mask **M1**) and oxidation sharpening. Details of this step and the general strategy for the complex tip formation are given in Section IV. A conformal, low stress, 0.25–0.30-μm -thick silicon nitride film is deposited by low-pressure chemical-vapor deposition (LPCVD) to form the floor of the channels. Mask **M2** defines the space where the on-chip reservoir will connect to the channels. A sandwich of silicon oxide (0.4–0.5 μm thick, low temperature oxide, LTO) and low stress silicon nitride (0.3–0.5 μm thick) are deposited by LPCVD, to form the sacrificial layer and the ceiling layer of the microchannels. Lithography with mask **M3**, followed by reactive ion etching (RIE) in CF_4 plasma, define the channels' in-plane geometry. The channels follow the edges of the pattern comprised in mask **M3**, as

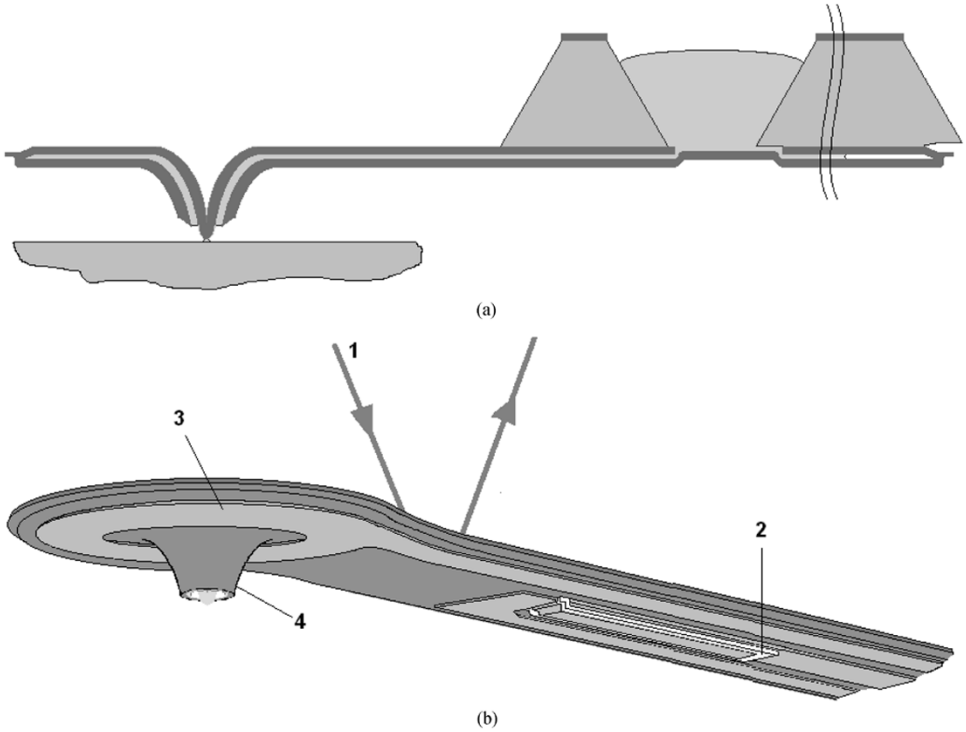

Fig. 2. General view of microfluidic nanoprobe. (a) Cross-sectional view showing microfluidic components, from reservoir to tip; (b) 3-D schematic view of the cantilever, showing 1—laser beam from AFM position sensor, 2—piezoactuator, 3—electrode for applying pressure pulses, 4—microfluidic volcano tip. Note: 2 and 3 are in development stages and here discussed only from a design viewpoint.

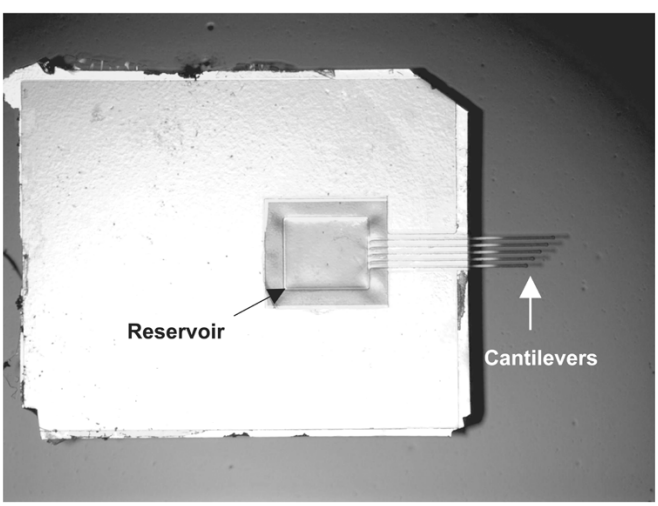

Fig. 3. General view of microfabricated chip. Dimensions are: 2.66 mm $\times$ 3.27 mm (chip excluding cantilevers), 810 μm $\times$ 891 μm (reservoir), and 400 to 600 μm (cantilevers). The size of the chip was chosen to fit in standard AFM equipment. The on-chip reservoir can be connected with a capillary tube to a separate larger reservoir, or the reservoir can be directly filled and capped.

will be described in Section III. A buffered oxide etching solution (BOE) is used for a controlled underetching of the structures, to provide the lumen of the microchannels. The next steps are closing the lateral openings of the channels by a *bird's beak* oxidation and sealing by deposition of an additional silicon nitride layer (LPCVD or sputtered, 0.2–0.3 μm thick).

The material of the sealing layer is not essential if some requirements regarding compatibility with the process and stress budget are respected. As will be discussed in Section III, usage of other materials is possible. These include metals, e.g., gold (e-beam evaporated or sputtered, 0.3–0.4 μm thick), which may be useful for component integration purposes. In Fig. 1(f)–(h), silicon nitride is shown, as used in our experiments. Lithography with mask **M4** is used to pattern the sealing layer with the geometry of the cantilevers and chip boundaries. Backside alignment of mask **M5**, patterning the backside nitride by CF_4 RIE, and KOH etching are used to form the reservoir and shape the solid body of the chip. This step requires convex corner compensation structures, which will be discussed in Section IV. After the removal of the oxide in step h, the chip remains suspended by small, easy-to-break silicon bridges, for providing good wafer-level maneuverability. After this step, a thin Cr/Au layer (5 nm/ 15 nm) is deposited on the back side of the wafer, to provide sufficient reflectivity from the cantilevers for the AFM laser position sensor.

After release, the chip is supposed to work as illustrated in Fig. 2(a). To diminish the evaporation of the ink solvent, a polydimethylsiloxane (PDMS) cap was used to cover the backside of the reservoir. Alternatively, the on-chip reservoir can be connected with a capillary tube to a separate larger reservoir. The chip designed so far works as a five-probe device, mounted in standard AFM equipment, with no independent actuation of the cantilevers. However, we designed the device having in mind several possible actuation mechanisms. The actuation can be easily integrated on the tip-side of the cantilever, with additional processing between steps f and g in the flowchart. Thermal actuation, although simple and well established, is probably not the best choice, since temperature may interfere with molecular flow, accelerate evaporation and modify the diffusion properties of the ink. Thus, a piezoelectric actuation is presently under experimentation, as shown in Fig. 2(b). Additional electrodes can

TABLE II
MAIN PARAMETERS OF THE TWO LPCVD SILICON NITRIDE FILM DEPOSITIONS

Parameter\ Material	Dichloro-silane flow (sccm/min)	Ammonia flow (sccm/min)	Deposition Temperature (°C)	Pressure (mTorr)	Residual /thermal /Intrinsic stress (MPa)
Low stress nitride	60	14	875	205	120/450/-330
High stress nitride	22	93	805	205	1300/2503/-1150

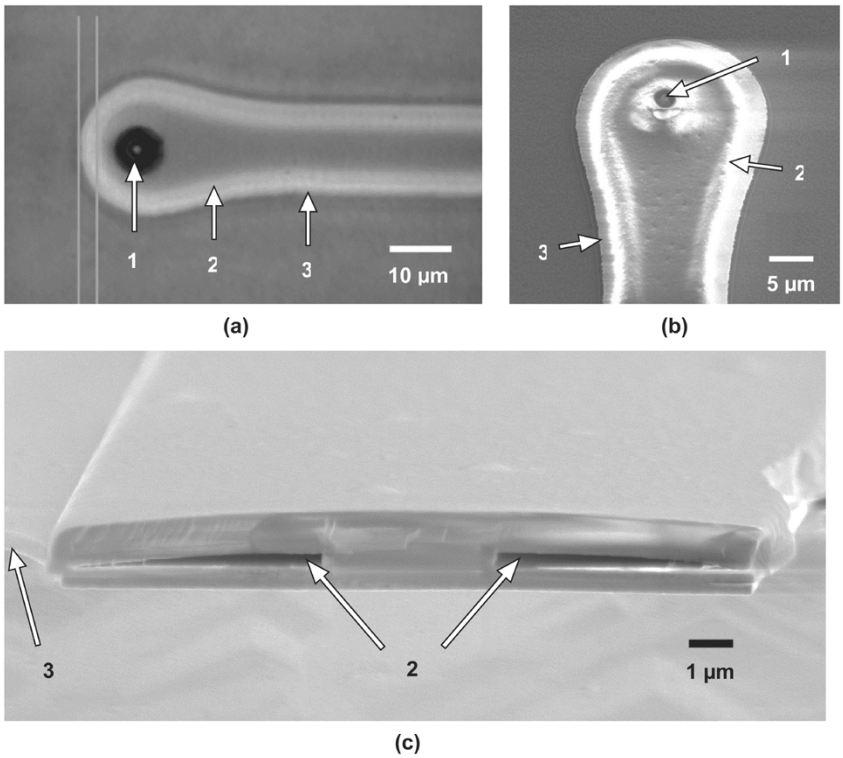

Fig. 4. (a) Optical micrograph of a structure with sealed microchannels following the outer edge of the cantilever. (b) SEM of a free-standing cantilever with channels and connected volcano tip. (c) Cross section SEM view of the channel structure. The cantilever was cut transversally by a focused ion beam (FIB). 1—volcano tip; 2—microchannels; 3—sealing layer.

be provided for other purposes, such as for electrochemistry applications or for applying short local, voltage-controlled pressure pulses at the end of the cantilever, to wet or clean the tip if necessary [Fig. 2(b)].

III. FABRICATION OF MICROCHANNELS

Several criteria were used to select fabrication processes employed in the fabrication of microchannels: capability to integrate them in cantilevers with minimum stiffness, microfluidic compatibility with ink solutions (size, contact angle, easiness to clean after the release of the sacrificial core material over long distances), simplicity in microfabrication, and compatibility with other processes and future augmentations. After evaluating several options of channel fabrication methods from the literature [27]–[30], we adopted a novel method [see Fig. 1(d)–(g)], which uses one mask less and requires a thinner sealing layer than the best-suited procedure found in the literature [30]. In order to achieve a good closure of the gap, while having a suited lumen thickness (0.3–0.5 μm), besides the *bird's beak* technique, the ceiling nitride deposition technique was modified to build in a gradient of stress to induce a transversal bending. This was done by performing a two step deposition: a first 50 nm of high-stress nitride was deposited (1200 MPa tensile stress), followed by a 150 nm of low stress nitride (200 MPa tensile). The stress levels reported here were measured on separate test wafers using a Tencor FLEXUS 2320 wafer curvature measuring system. The LPCVD deposition parameters are given in Table II.

The Si_3N_4 sealing layer had again to be stress engineered, to prevent the longitudinal bending of the cantilevers. With a low-stress LPCVD nitride as sealing layer, the general trend was that the cantilevers bended down after their release. The bending curvature for this case was measured using scanning electron microscopy (SEM) and the thickness of a high stress nitride was calculated to replace the low stress nitride for sealing and compensate the longitudinal bending. Both the calculations and the practical results confirmed that a 300-nm-thick high-stress nitride was the solution. A slight bending of the cantilevers ($\sim 1.4^{\circ}$ at the end for the 500-μm-long cantilever) toward the tip side was found beneficial for the probe geometry, since it brought the tip about 12 μm out of the chip plane, useful for

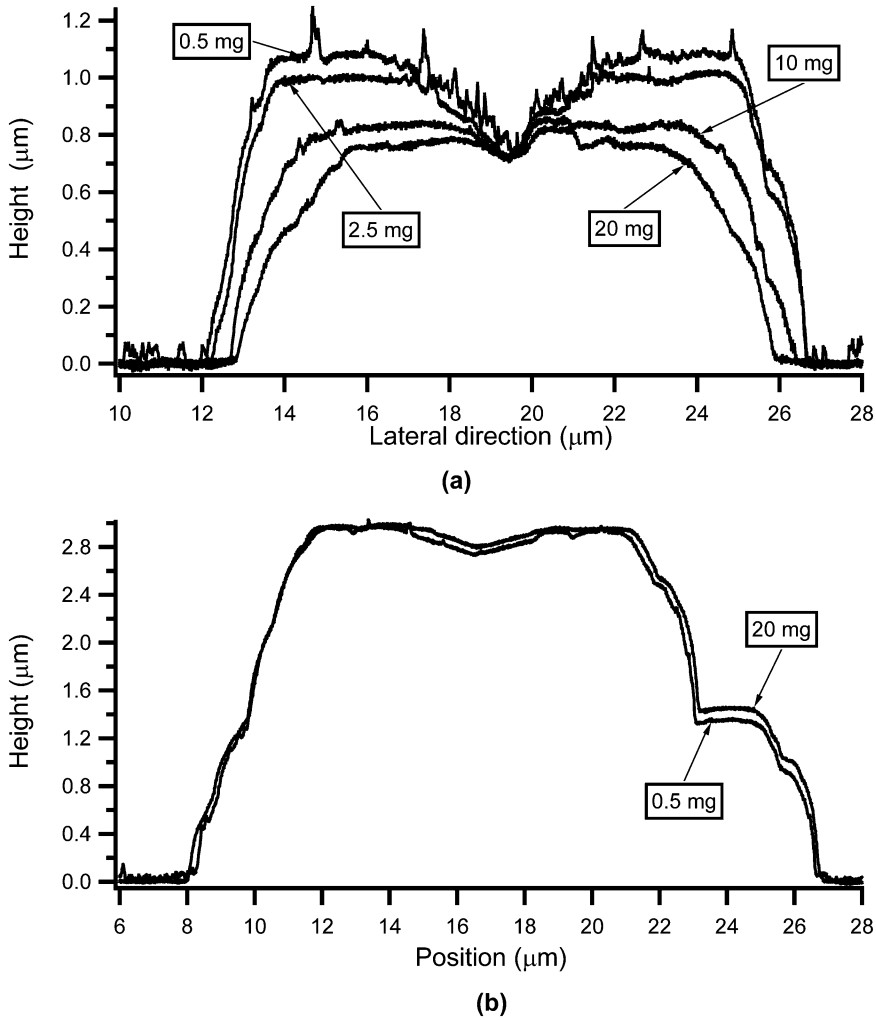

Fig. 5. Mechanical profilometry scans (Tencor Alphastep 500) across the microchannel structure before *bird's beak* oxidation (a) and after oxidation, sealing with LPCVD nitride and patterning the cantilevers with mask M4 (b). While increasing the stylus force, before the oxidation one can notice the lowering of the side wings of the ceiling layer, while after sealing, no deformation can be noticed. The inequality of the left and right shoulders in b) is due to a slight mask misalignment of $\sim 1\ \mu\mathrm{m}$ for patterning the sealing layer.

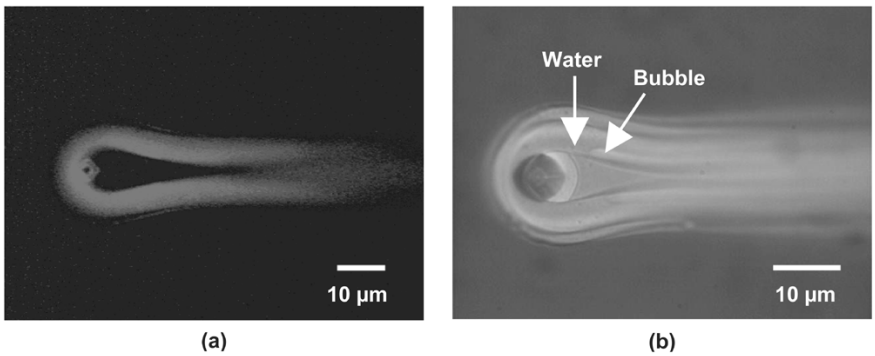

Fig. 6. (a) Fluorescence optical microscopy image of the microchannels filled with a solution of Texas red dye in DI water, (b) optical microscopy image of the microchannels, surrounding the volcano tip, showing an air bubble formed from the high evaporation rate caused by heating from the microscope light.

mounting the chip into the AFM. Fig. 4 shows a top and cross sectional view of a sealed microchannel. Other cantilever details can be seen in Figs. 3, 6, and 7(c), (d).

As discussed above, for future integration of independent actuation or for providing an electrode for electrochemical experiments, the sealing layer may be chosen to be a medium or low conformity evaporated or sputter-deposited metal (Pt, Au, Ni). However, the control of residual stress in the metal films is less straightforward and the high thermal expansion coefficient of metals may render the beam curvature highly environment-dependant.

The proper closure of the channels before and after the sealing layer deposition was tested by mechanical profilometry, i.e., by scanning across the cantilevers with low (0.5 mg) and high

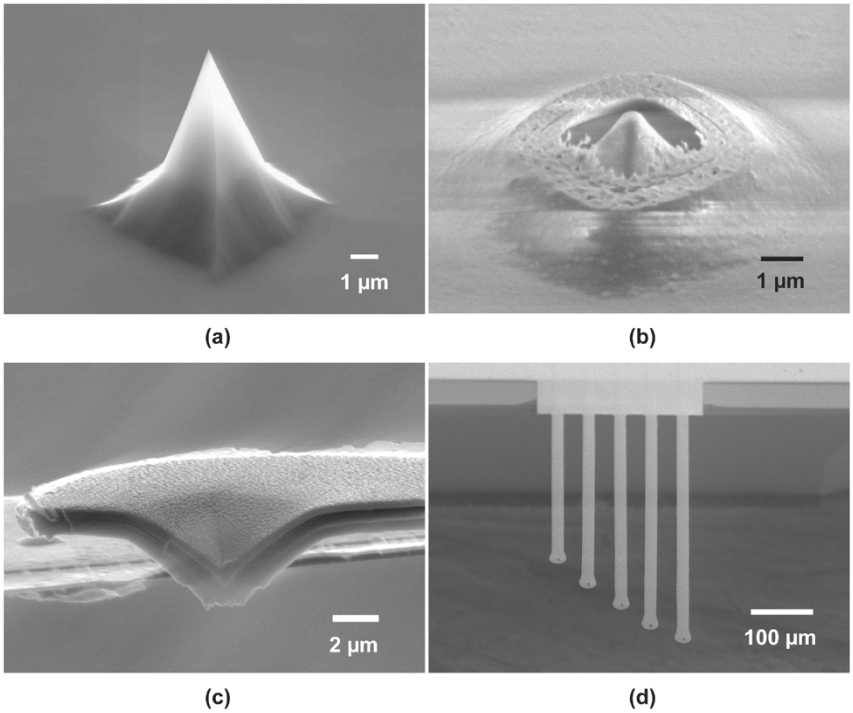

Fig. 7. Volcano tip formation: (a) precursor obtained by KOH and isotropic etching, (b) volcano structure, (c) SEM image of volcano tip cross section, obtained by focused ion beam with a cut not made exactly across the tip center, showing good connectivity between microchannel and tip apex, and (d) SEM image of released cantilevers with tips.

(20 mg) tip forces. The results are plotted in Fig. 5. Fig. 5(a) shows the profiles at various contact forces prior *bird's beak* oxidation. As expected, deflection of the channel ceiling layer is observed. By contrast, after oxidation and sealing, no noticeable difference in the profiles are observed when contact loads of 0.5 mg and 20 mg are employed. Should the gap closure or sealing be imperfect, a difference between the low and high force profiles should be observed. Tests after the sealing layer deposition step were also performed by examining the channels in reflection mode with an optical microscope and by dipping them into deionized (DI) water or acetone. Note that the channels shouldn't be flooded by the liquids before the final chip release, but should be filled due to capillary action after release. Final connectivity tests after chip release were performed with a DI water-diluted fluorescent dye (Texas Red, Dextran). The experiments showed a good penetration of the dye along the entire path of the channels, from the reservoir to the tips. Fig. 6(a) shows a fluorescence optical micrograph of the channels flooded by the dye solution fed from the reservoir. Similar results were obtained by feeding DI water, to visualize the meniscus moving through the channels, and examining the cantilevers with an optical microscope. In this case, air bubbles were observed to develop in the channels, near to the tips, due to the fast evaporation rate caused by the microscope illumination [see Fig. 6(b)]. These experiments proved that there is good fluidic connectivity between reservoir and tips all the way through the microfluidic channel system.

IV. Fabrication of the Volcano Tips

The fabrication of the tips starts with the patterning of the tip precursors [see Fig. 1(a)]. The masking layer was usually low stress silicon nitride, but good results were obtained also with thermal oxide. Mask **M1** contained seven groups of precursors of different sizes, associated to different alignment marks, such that the fabrication could be continued with mask **M2** on any of the desired groups. Several etching agents were tried, resulting in various heights and geometries of tips. Finally, a combination of KOH etching (starting from square masks with compensation beams, as described by Ofereins *et al.*, [31]), followed by a short isotropic Si etching with a HF-HNO_3-CH_3COOH (3:5:3) mixture for controlled sharpening were selected as best suited. Final sharpening by growing a 1-μm-thick low temperature thermal oxide (950°C) led to tips radii in the range of 5–20 nm. The fabrication of the volcano tips followed the scheme presented in Fig. 1 and the outcome can be viewed in Fig. 7. A critical step was the formation of the volcano structure, in step g, by CF_4 RIE (50 mTorr, 100 W, 50 sccm, in an Oxford Instruments MP 80 RIE system). A good control over the resist thickness and differential etching rates of photoresist and nitride were essential.

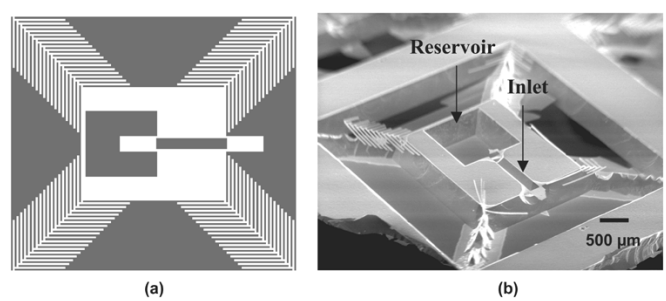

Fig. 8. (a) Mask with compensation structures and (b) released chip. Convex corner compensation beams were used for protecting the chip corners and the inlet and outlet corners of the V-grove channel.

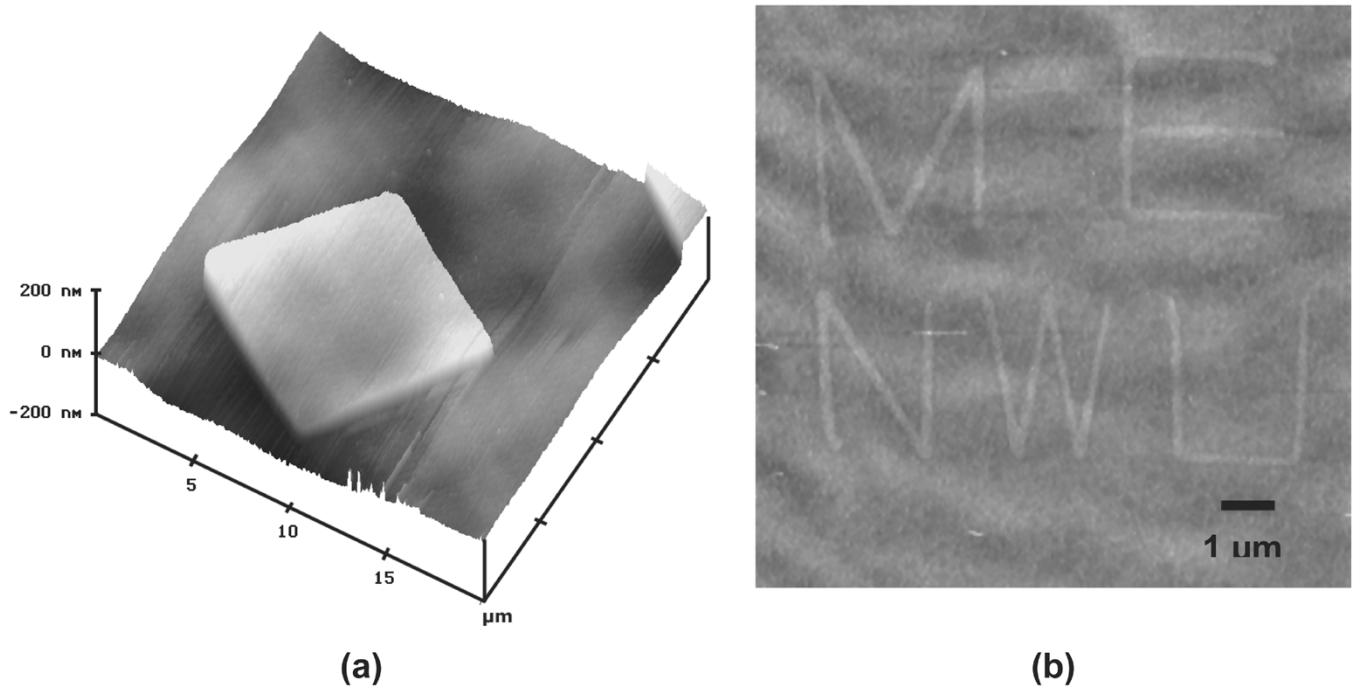

Fig. 9. (a) Contact mode AFM image, of a calibration standard, recorded with the new probe, and (b) Pattern obtained with the new probe in DPN mode writing with MHA molecular ink self-assembled on a gold substrate.

The tip etching had to stop after reaching the sacrificial oxide layer, but the level of the volcano shell-nitride had to be also lower than the core volcano nitride dome. This was achieved by choosing appropriate resist thickness and thermal treatment. A resist thickness of 3.8 μm (S 1818, Microchem Co.), starting with 5-μm-heigh silicon tips generally provided good results. Fig. 7(b) and (c) show features of the tip after etching of the sacrificial oxide layer. Good connectivity between microchannels and tips was observed.

The fabrication process described so far is able to produce tips with radii larger or equal to the bottom nitride layer thickness (250 nm), which is far from the performance of regular AFM tips, but is a good result for coated tips. To overcome this limitation, several solutions are investigated and will be reported in future manuscripts.

V. Fabrication of Reservoir and Chip Body

The chip body formation required convex corner compensation structures. A general view of the back side mask layout and the final etching outcome are shown in Fig. 8. The chip corners are protected by compensation beams of the type described in [31], which were optimized for a KOH etching solution of 30%, working at 80 °C. A V-grove channel was included on the backside of the chip, for creating a ventilation path to prevent the stopping of the fluid flow by underpressure, after reservoir capping. Alternatively, the V-grove channel can be used to connect a 100-μm outer diameter capillary tube to a remote reservoir. In fact, we have conducted such experiments satisfactorily to investigate microchannel sealing under pressure. In this case, we have glued a solid glass cap and a capillary tube to the backside of the chip. Using a syringe we filled the reservoir. Note that the corners of the V-grove channels are also protected from convex corners underetching by two rectangular compensation structures, Fig. 8(a). After release by KOH etching, the chip remained suspended on four silicon beams, attached to its corners, and the V-groove inlet had the desired shape, see Fig. 8(b).

VI. Functional Tests and Results

Several tests have been performed to check the writing and reading capabilities of the novel probes. Chips were mounted into a Dimension 3100 AFM (Digital Instruments). One of the five cantilevers was set in the optical path between the laser and four quadrant detector. The signal was employed for feedback-contact detection by the AFM. Imaging in constant force mode was tested on a calibration standard (Pacific Nanotechnology), consisting of an array of squares, with different lateral sizes in the 1–10 μm range, and heights of 80 nm. The imaging capabilities of the fountain pen probes in tapping and contact modes were completely similar to those of standard AFM probes (VEECO, NP-20) even when tip radii where quite different. This is likely due to the development of roughness features, such as small spikes, during the reactive ion etching step used to expose the tips, step (g) in Fig. 1. In lateral force mode, our probes outperformed the standard probes in resolution and sensitivity as a result of the lower torsional stiffness of the designed cantilevers.

The first writing tests were performed in standard DPN mode, using ODT and MHA solutions. For these tests, the ink molecules were supplied both by evaporation from a heated source and by dipping the tips in a liquid droplet. Fig. 9 shows a contact mode image of the calibration structure and a lateral force mode image of patterns written with the same tip using MHA as ink and a freshly-deposited gold film as substrate. The writing of the letters was done at 0.03 μm/s scan rate and

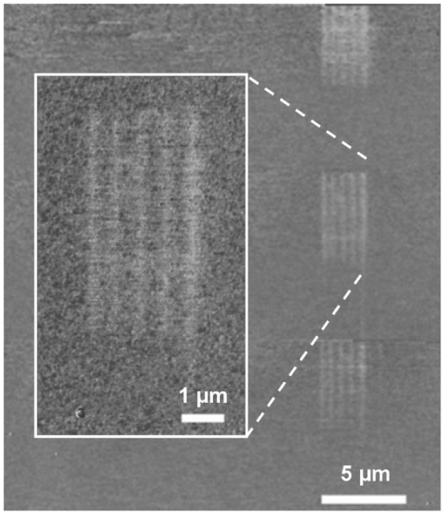

Fig. 10. Lateral force image of arrays of lines written with 16-mercaptohexadecanoic acid (MHA) deposited onto a gold substrate by supplying molecular ink solution from the reservoir through the microchannels. Line widths in this picture are ~ 150 nm, but lines as fine as 40 nm were obtained [32].

60% relative humidity. These tests proved that the developed fountain probes do not exhibit material or fabrication-related incompatibility for DPN mode writing and reading of molecular inks.

Writing by supplying the ink from the reservoir, with fluid transport through the microchannels to the tip apex was also tested with positive results. Ink was supplied by placing a droplet of 1 mM MHA solution in ethanol into the reservoir, after which the reservoir was capped with a PDMS sheet placed onto the chip using tweezers. Subsequently, the chip was mounted carefully into the same AFM head as for the previous tests, and the writing on a gold substrate was performed with a sweeping speed of 0.05 $\mu\mathrm{m/s}$ at room temperature in a 60% relative humidity environment. The line width obtained with this speed usually was under 150 nm for most of the probes tested (Fig. 10). An unprecedented resolution of 40 nm was also achieved with one probe [32]. Similar to the DPN technique [19], factors such as temperature, relative humidity, chemical nature of the ink and substrate, and writing speed were found to affect the writing resolution of the actual probes too. To them, we may add the curvature radius and geometrical configuration of the tips, which is variable in some degree due to the fabrication process, and due to wear/pick up of particles during the writing/reading processes. As mentioned, the apex radii for all these tips were nominally 250 nm, which suggests that local roughness features contribute to this high resolution both in imaging and writing.

The reported writing test was generally performed 5–10 min after feeding the ink into the reservoir. Observation of the ink drying process in the reservoir of unmounted chips showed that the ink remains in liquid state for about 12 min. Tips with longer hold times before writing, also performed well (dried ink).

VII. Conclusion

A novel type of microfluidic nanoprobe suited for continuous writing in fountain-pen lithography mode has been designed and fabricated. It consists of special dispensing volcano AFM tips, integrated with cantilevers containing embedded microchannels. These microchannels connect the volcano tips to an on-chip reservoir. The reservoir can be further connected to a larger, remote reservoir, via a capillary tube, or simply capped. A novel procedure was employed for the fabrication of microchannels, consisting of edge underetching a sandwiched nitride/oxide/nitride tri-layer, *bird's bea*k oxidation and sealing. The new technique permits easy integration of the channels into low-stiffness cantilevers, preserves the geometry and cleanliness of the lumen over hundreds of microns, requires fewer masks than previous procedures and is well suited for arraying the cantilevers. Writing tests in "fountain pen mode" show the microfluidic tip preserves the dip-pen diffusion-driven writing in the proximity of the tip. Patterns with a width resolution of 40 to 150 nm have been achieved. The probe performs very well in AFM lateral force and contact imaging modes, which allows writing and reading with the same chip. Our primary interest in this manuscript is to show that the novel probes can use a liquid source and write in "fountain mode". However, long-run writing experiments and comparison with traditional DPN mode should be pursued. Such experiments will require continuous feeding, through a capillary tube attached to the chip, to feed ink into the reservoir and prevent drying during longer writing processes.

Several enhancements currently underway were also discussed. They include formation of sharper tips, independent cantilever actuation and integration of metal electrodes. This design has the potential to be arrayed and can revolutionize the way organic and inorganic molecules are deposited and manipulated on surfaces for a large number of nanotechnology applications and fundamental studies.

Acknowledgment

Any opinions, findings, and conclusions or recommendations expressed in this material are those of the author(s) and do not necessarily reflect those of the National Science Foundation. The authors would like to thank Chad Mirkin and his group of students and post-docs for many insightful discussions on DPN. The authors acknowledge the Microfabrication Applications Laboratory (MAL) of the University of Illinois at Chicago, the Materials Processing and Crystal Growth Facility (MPCGF) of Northwestern University, and Northwestern University Atomic- and Nanoscale Characterization Experimental Center (NU*ANCE*) for the fabrication and characterization facilities.

References

[1] J. A. Jarrell, J. G. King, and J. W. Mills, "A scanning micropipette molecule microscope," *Science*, vol. 211, pp. 277–279, Jan. 1981.

[2] P. K. Hansma, B. Drake, O. Marti, S. A. C. Gould, and C. B. Prater, "The scanning ion-conductance microscope," *Science*, vol. 243, pp. 641–643, Feb. 1989.

[3] A. Lewis, Y. Kheifetz, E. Shambrod, A. Radko, and E. Khatchatryan, "Fountain pen nanochemistry: Atomic force control of chrome etching," *Appl. Phys. Lett.*, vol. 75, no. 17, pp. 2689–2691, Oct. 1999.

[4] M.-H. Hong, K. H. Kim, J. Bae, and W. Jhe, "Scanning nanolithography using a material-filled nanopipette," *Appl. Phys. Lett.*, vol. 77, no. 16, pp. 2604–2606, Oct. 2000.

[5] I. W. Rangelow, J. Voigt, and K. Edinger, ""Nanojet": Tool for the nanofabrication," *J. Vac. Sci. Technol. B*, vol. 19, no. 6, pp. 2723–2726, Nov./Dec. 2001.

[6] S. Shalom, K. Lieberman, A. Lewis, and S. R. Cohen, "A micropipette force probe suitable for near-field scanning optical microscopy," *Rev. Sci. Instrum.*, vol. 63, no. 9, pp. 4061–4065, Sep. 1992.
[7] I. Papautsky, J. Brazzle, H. Swerdlow, R. Weiss, and A. B. Frazier, "Micromachined pipette arrays," *IEEE Trans. Biomed. Eng.*, vol. 47, no. 6, pp. 812–819, Jun. 2000.
[8] S. Chandrasekaran, J. D. Brazzle, and A. B. Frazier, "Surface micromachined metallic microneedles," *J. of Microelectromechanical Systems*, vol. 12, no. 3, pp. 281–288, Jun. 2003.
[9] K. T. Brown and D. G. Flaming, *Advanced Micropipette Techniques for Cell Physiology*. New York: Wiley, 1986.
[10] Y. Shao, M. D. Osborne, and H. H. Girault, "Assisted ion transfer at micro-ITIES supported at the tip of micropipettes," *J. Electroanal.Chem.*, vol. 318, pp. 101–109, 1991.
[11] G. Taylor and H. H. J. Girault, "Ion transfer reactions across a liquid-liquid interface supported on a micropipette," *J. Electroanal. Chem.*, vol. 208, pp. 179–183, 1986.
[12] R. D. Piner, J. Zhu, F. Xu, S. Hong, and C. A. Mirkin, "Dip-pen" nanolithography," *Science*, vol. 283, pp. 661–663, 1999.
[13] S. Hong, J. Zhu, and C. A. Mirkin, "Multiple ink nanolithography: Toward a multiple-pen nano-plotter," *Science*, vol. 286, pp. 523–525, Oct. 1999.
[14] A. Ivanisevich and C. A. Mirkin, "Dip-Pen" nanolithography on semiconductor surfaces," *J. Amer. Chem. Soc.*, vol. 123, pp. 7887–7889, 2001.
[15] K.-B. Lee, S.-J. Park, C. A. Mirkin, J. C. Smith, and M. Mrksich, "Protein nanoarrays generated by dip-pen nanolithography," *Science*, vol. 295, pp. 1702–1705, Mar. 2002.
[16] P. Gould, "Lithography: Rewriting the rules," *Mater. Today*, pp. 34–39, 2003.
[17] J. Jang, S. Hong, G. C. Schatz, and M. A. Ratner, "Self-assembly of ink molecules in dip-pen nanolithography: A diffusion model," *J. Chem. Phys.*, vol. 115, pp. 2721–2729, Aug. 2001.
[18] P. E. Sheehan and L. J. Whitman, "Thiol diffusion and the role of humidity in "dip-pen nanolithography"," *Phys. Rev. Lett.*, vol. 88, pp. 156 104-1–156 104-4, Apr. 2002.
[19] S. Rozhok, R. Piner, and C. A. Mirkin, "Dip-pen nanolithography: What controls ink transport," *J. of Physical Chemistry B*, vol. 107, pp. 751–757, 2003.
[20] Y. Li, B. W. Maynor, and J. Liu, "Electrochemical AFM "dip-pen" nanolithography," *J.Am.Chem. Soc.*, vol. 123, pp. 2105–2106, 2001.
[21] P. Vettiger, M. Despont, U. Drechsler, U. Durig, W. Haberle, M. I. Lutwyche, H. E. Rothuizen, R. Stutz, R. Widmer, and G. K. Binnig, "The "Millipede"—More than thousand tips for future AFM data storage," *IBM J.Res. Develop.*, vol. 44, pp. 323–340, May 2000.
[22] M. Zhang, D. Bullen, S.-W. Chung, S. Hong, K. S. Ryu, Z. Fan, C. A. Mirkin, and C. Liu, "A MEMS nanoplotter with high-density parallel dip-pen nanolithography probe arrays," *Nanotechnol.*, vol. 13, pp. 212–217, 2002.
[23] D. Bullen, X. Wang, J. Zou, S. Hong, S.-W. Chung, K. Ryu, Z. Fan, C. Mirkin, and C. Liu, "Micromachined arrayed dip pen nanolithography probes for sub-100 nm direct chemistry patterning," in *Proc. 16th IEEE International Micro Electro Mechanical Systems Conference, MEMS 2003*, Kyoto, Japan, Jan. 19–23, 2003, pp. 4–7.
[24] K.-H. Kim, C. Ke, N. Moldovan, and H. D. Espinosa, "A novel AFM chip for fountain pen nanolithography—Design and microfabrication," in *Materials Research Society Symposium Proceedings*, vol. 782, 2003, pp. A5.56.2–A5.56.6.
[25] H. D. Espinosa, N. Moldovan, and K.-H. Kim, "US Patent Application," USSN 60/4 55 89 8, Mar. 19, 2003.
[26] R. D. Piner and C. A. Mirkin, *Effect of Water on Lateral Force Microscopy in Air*: Langmuir, 1997, vol. 13, pp. 6864–6868.
[27] M. J. de Boer, R. W. Tjerkstra, J. W. Berenschot, H. V. Jansen, G. J. Burger, J. G. E. Gardeniers, M. Elwenspoek, and A. l. van den Berg, "Micromachining of buried micro channels in silicon," *J. Micorelectromech. Syst.*, vol. 9, pp. 94–103, 2000.
[28] L. Quellet and H. Tyler, "Manufacture of Integrated Fluidic Devices," U.S. Patent 2002/0 160 561 A1, Oct. 31, 2002.
[29] S. D. O'Connor and E. Dantsker, "Microfluidic Devices for Heat Transfer," U.S. Patent 6 501 654 B2, Dec. 31, 2002.
[30] V. B. Kley, "Monolithic Fabrication of Fluidic Structures," International Patent WO 00/42 233, Jul. 20, 2000.
[31] H. L. Offereins, H. Sandmaier, K. Marusczyk, K. Kuhl, and A. Plettner, "Compensating corner undercutting of (100) silicon in KOH," *Sens. Mater.*, vol. 3, pp. 127–144, 1992.
[32] K.-H. Kim, N. Moldovan, and H. D. Espinosa, "A nanofountain probe with sub-100 nm molecular writing resolution," *Small*, vol. 1, pp. 632–635, 2005.

Nicolaie Moldovan received the Master's and Ph.D. degrees in physics from the University of Bucharest, Romania, and completed several research stages in the Fraunhofer Institute for Solid State Technology Germany, IMM Mainz, and LASS/CNRS Toulouse.

He held the position of senior researcher and head of the Non-Conventional Microfabrication Laboratory for several years in the Romanian Institute for Microtechnology, where he run projects in silicon and glass micromachining, atomic-scale simulation of etching, microoptics and LIGA. During 1998-2002, he joined Argonne National Laboratory, where he developed ultra-deep (1 cm) LIGA technology, tilted/dynamic X-ray exposure techniques and micromachining techniques for new materials, such as ultra-nanocrystalline diamond, and applications such as X-ray microoptics, microfluidics, field emitters and various microelectromechanical systems. He signed more than 100 scientific papers. His special professional interest relies on micro- and nanodevices for experiments leading to a better understanding of fundamental laws governing phenomena at these scales.

Keun-Ho Kim received the B.S. and M.S. degrees in mechanical engineering from Hanyang University, Seoul, Korea, in 1996 and 1998, respectively. He is currently working towards the Ph.D. degree in the Department of Mechanical Engineering, Northwestern University, Evanston, IL.

His research interests include design, fabrication, and testing of MEMS/NEMS.

Horacio D. Espinosa received the degree in civil engineering from Universidad Nacional del Nordeste, Argentina, in 1981, the M.Sc. degree in structural engineering from Politecnico di Milano, Italy, in 1987, and the Ph.D. degree in applied mechanics from Brown University, Providence, RI, in 1992.

Currently, he is Professor of Mechanical Engineering at Northwestern University, Evanston, IL. After receiving his Ph.D. degree, he joined the Purdue University faculty and later moved to Northwestern University in 2000. He has made contributions in the areas of dynamic failure of advanced materials, micro- and nanomechanics. He has published over 100 technical papers in these fields. Professor Espinosa has received numerous awards and honors recognizing his research and teaching efforts, including two Young Investigator Awards, NSF-Career and ONR-YIP, the Hetenyi Award from the SEM, and the American Academy of Mechanics (AAM) Junior Award.

Dr. Espinosa is a Fellow of the AAM, ASME, and past Editor of Mechanics, a publication of AAM. He currently serves as Associate Editor of the *Journal Experimental Mechanics* and the *Journal of Applied Mechanics*. His research interests are on dynamic failure of materials, size scale plasticity and fracture of thin films and MEMS/NEMS materials, *in situ* electron and atomic probe microscopy testing of nanoobjects, failure mechanisms in biomaterials such as nacre and abalone shells, and the development of devices for massively parallel atomic probe writing with chemicals and biomolecules.